Andreev Reflection versus Coulomb Blockade in Hybrid Semiconductor Nanowire Devices

Yong-Joo Doh,[†,⊗] Silvano De Franceschi,*[,‡,§] Erik P. A. M. Bakkers,[∥] and Leo P. Kouwenhoven[†]

Kavli Institute of Nanoscience, Delft University of Technology, P.O. Box 5046, 2600 GA Delft, Netherlands, National CRI Center for Semiconductor Nanorods, POSTECH, Korea, CEA, INAC/SPSMS/LaTEQS, 17 Rue des Martyrs, 38054 Grenoble, France, CNR-INFM, Laboratorio Nazionale TASC, S.S. 14, Km 163.5, 34012 Trieste, Italy, and Philips Research Laboratories, Professor Holstlaan 4, 5656 AA Eindhoven, Netherlands

ABSTRACT

Semiconductor nanowires provide promising low-dimensional systems for the study of quantum transport phenomena in combination with superconductivity. Here we investigate the competition between the Coulomb blockade effect, Andreev reflection, and quantum interference, in InAs and InP nanowires connected to aluminum-based superconducting electrodes. We compare three limiting cases depending on the tunnel coupling strength and the characteristic Coulomb interaction energy. For weak coupling and large charging energies, negative differential conductance is observed as a direct consequence of the BCS density of states in the leads. For intermediate coupling and charging energy smaller than the superconducting gap, the current−voltage characteristic is dominated by Andreev reflection and Coulomb blockade produces an effect only near zero bias. For almost ideal contact transparencies and negligible charging energies, we observe universal conductance fluctuations whose amplitude is enhanced because of Andreev reflection at the contacts.

In recent years, semiconductor nanowires (NWs) have attracted a lot of attention because of their potential for applications in the domain of nanoscale sensors, electronics, and photonics.[1] Simultaneously, the highly controlled synthesis of homo- and heterostructured NWs has provided a new platform to study fundamental quantum phenomena and develop novel quantum devices.[2] Resonant tunneling[3] and Coulomb blockade[4–6] behavior have been observed in the low-temperature electronic transport[7] of individual NWs. Also, NWs have been efficiently connected to conventional superconductors (SCs), leading to the observation of gate-tunable supercurrents,[8,9] π-junction behavior,[10] and Kondo-enhanced Andreev tunneling.[11] Although in all of these experiments the NW-SC tunnel coupling ranged between moderate and strong, less attention has been paid to the weak coupling limit, where the characteristic energy scales associated with the Coulomb blockade effect and with size quantization largely exceed the superconducting energy gap.

This regime was addressed for the first time by Ralph et al.[12] who could obtain quantum dots weakly coupled to SCs by embedding metallic nanoparticles in a thin oxide layer sandwiched between two SC contacts. In this pioneering work, negative differential conductance (NDC) was observed as a hallmark of the BCS density of states (DOS) in the source/drain electrodes.[13,14] Further studies of the dependence on particle size or tunnel coupling, however, were hindered by experimental difficulties in the device fabrication process. Other more recent attempts using either carbon nanotubes[15] or self-assembled InAs nanocrystals[16] lacked clear evidence of NDC.

In this Letter, we report an extensive study of SC-NW-SC hybrid systems embracing a wide range of contact transparencies, from very low to almost ideal ones. The observed transport properties are determined by an interplay of different mesoscopic phenomena with competing energy scales including *electron−electron Coulomb interactions*, characterized by a charging energy $E_c = e^2/C_\Sigma$ where e is the electron charge and C_Σ is the total capacitance of the NW; *Andreev reflection*, determined by the energy gap, Δ, of the superconducting electrodes; and *phase-coherent diffusive transport*, related to the Thouless energy, $E_{Th} = h/\tau_D$,

---

* Corresponding author. E-mail: silvano.defranceschi@cea.fr.
† Delft University of Technology.
⊗ National CRI Center for Semiconductor Nanorods.
‡ CEA, INAC/SPSMS/LaTEQS.
§ CNR-INFM, Laboratorio Nazionale TASC.
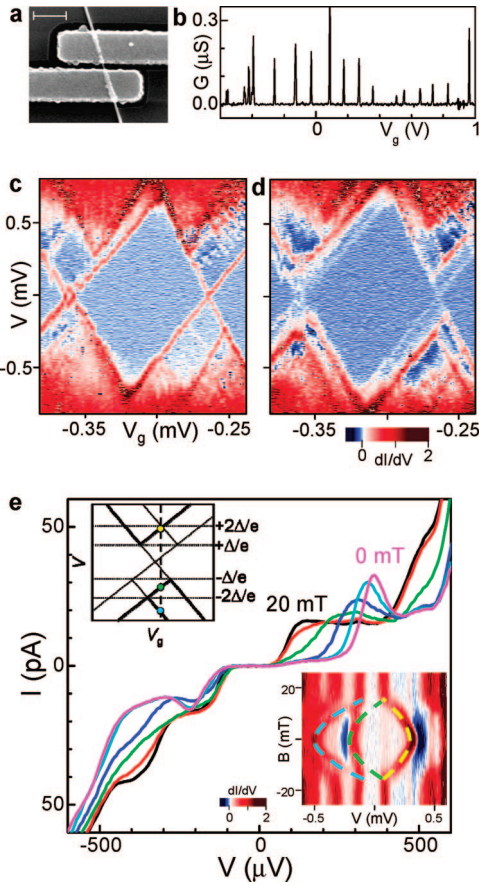∥ Philips Research Laboratories.

Figure 1. (a) Scanning electron micrograph of device **D1**, with interelectrode distance $L = 90$ nm and nanowire diameter $\phi = 36$ nm. Scale bar: 500 nm. (b) Back-gate voltage, V_g, dependence of linear conductance, G, at $T = 20$ mK under perpendicular magnetic field $B = 100$ mT (normal-state contacts). (c) Color plot of differential conductance, dI/dV, as a function of bias voltage, V, and V_g in the normal state ($B = 31$ mT) and (d) in the superconducting state ($B = 0$ mT). Dark-blue regions in part d) correspond to $dI/dV < 0$. (e) Current−voltage $I(V)$ characteristics at $T = 20$ mK, $V_g = -258$ mV, and $B = 20$ (black), 16 (red), 12 (green), 8 (blue), 4 (cyan), and 0 (magenta) mT. Lower inset: color plot of dI/dV versus (V, B) for the same T and V_g. Below the critical magnetic field of the contacts (~ 15 mT), the dI/dV peaks associated with the onset of single-electron tunneling shift according to the opening of a superconducting gap in the contacts (see dashed lines). Negative dI/dV is observed near $B = 0$ only for resonances associated with the source contact (yellow and green lines). The first drain-related resonance (blue line) exhibits a maximum V-shift of 0.37 mV (consistent with $\Delta = 0.14$ meV) but no negative dI/dV, suggesting a pronounced broadening in the BCS-like density of states of the drain contact. Upper inset: schematic view of stability diagram for the case of normal ($B = 31$ mT, thin solid lines) and superconducting ($B = 0$, thick solid lines) contacts. The vertical dashed line corresponds to $V_g = -258$ mV, and the colored circles indicate the observed dI/dV peaks at $B = 0$.

where h is Planck's constant and τ_D is the characteristic time an electron takes to diffuse along the entire NW length. We consider three limiting cases corresponding to clearly different coupling strengths between the NW and the SC contacts: (1) a weak tunnel coupling regime, with $k_B T \ll \Delta \ll E_c$ (T is temperature and k_B is Boltzmann's constant), in which transport is dominated by the Coulomb blockade phenomenon, and the superconducting nature of the electrodes manifests itself through its effect on their quasiparticle

density of states (DOS); (2) an intermediate coupling regime, with $k_B T \ll E_c \ll \Delta$, in which electronic transport is dominated by Andreev reflection and Coulomb blockade emerges only at low bias voltage; (3) a strong coupling regime, with $E_c \ll k_B T \ll \Delta$, E_{Th}, characterized by a combination of universal conductance fluctuations and Andreev reflection in the absence of Coulomb blockade.

The NWs employed for this work were synthesized by a vapor−liquid−solid process in which the semiconducting materials were supplied via laser ablation of n-doped InP or InAs targets. The NW growth was catalyzed by Au nanoparticles predeposited on a Si substrate. After growth, the NW's were dispersed in a chlorobenzene solution and deposited on a p^+ Si substrate with a 250-nm-thick SiO_2 overlayer. The SC contact electrodes were fabricated by e-beam lithography followed by the e-beam deposition of a Ti(10 nm)/Al(120 nm) bilayer. The NW surface was treated with buffered hydrofluoric acid for 20 s prior to metal evaporation. All low-temperature transport measurements were carried out in a dilution refrigerator equipped with accurately filtered wiring and low-noise electronics. Further details on NW growth, device fabrication, and measurement setup can be found in earlier publications.[4,8,17] The normal state resistance R_N, which we define as the dynamic resistance, dV/dI, at a bias voltage, V, of 1 mV and $T = 2$ K, was found to vary between ~ 1 to $\sim 10^3$ kΩ depending mostly on NW composition and diameter (see Table S1 and Figure S1 in the Supporting Information).

We consider first the device with the largest resistance, fabricated from a 36-nm-diameter InP NW (see Figure 1a). The device, labeled as **D1**, has $R_N/R_Q = 36$, where $R_Q = h/e^2 \sim 25.8$ kΩ is the resistance quantum. The NW channel forms a small quantum dot whose low-temperature transport properties are dominated by the Coulomb blockade effect over the whole experimental range, as denoted by the presence of characteristic quasi-periodic peaks[18] in the linear conductance, G (see Figure 1b). Such Coulomb peaks were measured at $T = 20$ mK under a perpendicular magnetic field of 0.1 T, large enough to suppress superconductivity in the Ti/Al electrodes. From the average peak-to-peak separation, $\delta V_g \sim 0.1$ V, we estimate a gate capacitance $C_g = e/\delta V_g \sim 2$ aF. On the basis of a simplified model (we use $C_g = 2\pi\epsilon_0\epsilon L_0/\ln(2h/r)$, where ϵ_0 is the vacuum permittivity, $\epsilon \sim 2.5$ is an effective dielectric constant accounting for presence of a SiO_2 layer under the NW and vacuum above it, L_0 is the length of the NW quantum dot, $h = 250$ nm is the thickness of the SiO_2 layer, and r is the NW radius) this C_g value corresponds to a dot length, $L_0 \sim 50$ nm, smaller than the source−drain distance $L = 90$ nm. This discrepancy can be ascribed to the electrostatic screening effect of the source and drain electrodes in such a short-channel device.[6]

More quantitative information on the NW quantum dot can be obtained from a measurement of the dynamic conductance, dI/dV, as a function of V_g, and V. The resulting stability diagram for normal leads is shown in Figure 1c. The height of the Coulomb diamonds yields $E_c \sim 0.7$ meV, corresponding to a total capacitance of the dot $C_\Sigma = C_s +$

$C_d + C_g \sim 230$ aF, where C_s and C_d are the capacitances of the source and drain tunnel junctions, respectively. Given a ratio $C_d/C_s \sim 1.6$, obtained directly from the slopes of the diamond edges,[19] we estimate $C_s = 88$ aF and $C_d = 140$ aF. The discrete energy spectrum of the NW quantum dot is revealed by the presence of additional lines parallel to the diamond edges. These lines are due to single-electron tunneling via the excited states of the dot, indicating a characteristic level spacing $\delta E = 0.2-0.3$ meV.[7]

The stability diagram changes dramatically as the magnetic field is turned off to revive superconductivity in the Ti/Al leads. As shown in Figure 1d, the Coulomb diamonds are split apart along the V axis, leading to the appearance of an almost "currentless window" around zero bias.[15] This window reflects the opening of superconducting gaps in the leads. In the case of ideal gaps with no quasiparticle states, current flow should be blocked all over the bias range between $-2\Delta/e$ and $2\Delta/e$. Figure 1d, however, displays two overlapping windows of suppressed conduction bound by $V = \pm 0.13$ and ± 0.26 mV, corresponding to $\pm\Delta/e$ and $\pm2\Delta/e$, respectively. Moreover, some weak conductance peaks can still be seen around zero bias at the charge-degeneracy points as a reminiscence of the diamond edges in the normal state. We ascribe these observations to the existence of quasiparticle states in the superconducting gap of the leads, which can be due to the granularity of the metallic contacts[20] and/or a nonzero DOS in the NW sections adjacent to the quantum dot.

For $|V| > \Delta/e$, the Coulomb peaks associated with the source lead (lines from the bottom left to the top right in Figure 1c and d) exhibit a sensible enhancement with respect to the normal case and they are followed by broader NDC lines (dark blue regions). We ascribe this combination of enhanced dI/dV peaks and NDC to a BCS-like DOS in the source electrode. The single-electron tunneling current has a maximum when the resonant dot level is aligned with the DOS peak at the edge of the superconducting gap, and it decreases at larger bias because of a reduction in the available DOS leading to NDC. This contrasts with the usual case of a quantum dot connected to normal leads where the available DOS is approximately constant and a quantum-dot level entering the bias window produces a step-like increase in the current, that is, a dI/dV peak with no NDC. (We note that another example of NDC was reported for NW resonant tunneling diodes and it was explained as an effect of the finite bandwidth of conduction electrons in the NW source lead.[3])

To illustrate the development of NDC resulting from the onset of superconductivity we show in Figure 1e, a set of $I(V)$ traces for a fixed gate voltage, $V_g = -0.26$ V, and different magnetic fields, from $B = 20$ mT to $B = 0$. In the normal state ($B = 20$ mT), the $I(V)$ exhibits the characteristic current steps expected for a constant DOS in the leads. Upon decreasing B, the current steps evolve into peaks leading to NDC. The gradual shift in the peak position toward larger $|V|$ reflects the increase in the superconducting energy gap. The quantitative relation between this shift, $\delta V(B)$, and $\Delta(B)$ can be obtained by taking into account the bias voltage division between the two tunnel junctions at the source and drain contacts. It can be shown that $\delta V = (C_s + C_d)\Delta/eC_s$ (or $(C_s + C_d)\Delta/eC_d$), when the initial tunneling step occurs through the drain (or source) junction.[12] Unlike in the experiment by Ralph et al.,[12] here all dot capacitances can be extracted directly from the Coulomb diamonds in Figure 1c without the need for multiparameter fits. From $C_d/C_s \sim 1.6$, we obtain $|\delta V| = 1.6\Delta$ and 2.6Δ for positive and negative V, respectively. Between $B = 20$ and 0 mT, we measure $\delta V = 0.22$ mV for $V > 0$, corresponding to $\Delta = 0.14$ meV, a value that is consistent with previous experiments.[8,22] For $V < 0$, the first resonance shows an anomalous shift of only 0.05mV. In ref 12, similar anomalous shifts were interpreted as a possible result of additional single-electron tunneling resonances via dynamically populated excited states. Here the anomaly has a simpler origin that can be understood by examining the B-evolution of the single-electron tunneling edges. As shown in the lower inset of Figure 1e and further clarified by the schematic stability diagram in the upper inset, the observed small shift originates from a resonance with the source and not with drain as one might expect.

We now consider the intermediate coupling regime with $R_N/R_Q \sim 1$ and $k_BT \ll E_c \ll \Delta$. Figure 2a shows a set of dI/d$V(V)$ characteristics at different temperatures for a device, **D2,** with channel length $L = 220$ nm, diameter $\phi = 44$ nm, and $R_N/R_Q = 0.77$. Below the superconducting transition temperature, $T_c \sim 1.3$ K, a conductance dip develops at low bias together with two peaks at $V = \pm2\Delta/e$. This behavior is typical of superconductor–insulator–normal metal–insulator–superconductor (SINIS) junctions in which conduction for $|V| < 2\Delta/e$ relies on Andreev reflection.[21] The fact that dI/dV in this Andreev-dominated range is suppressed with respect to the normal-state dI/dV (measured at high bias or for $T > T_c$) is due to a low transparency of the interfaces between the NW and the SC electrodes.[22]

An additional conductance dip appears at zero bias with a half-width $V_{HW} = 28$ μV at $T = 20$ mK. The depth of this dip is found to oscillate periodically with V_g as denoted by the oscillations in the linear conductance shown in Figure 2b. At $T = 20$ mK, these oscillations acquire the form of regularly spaced conductance peaks that can be fitted very well to a "classical" Coulomb blockade model,[18] $G/G_{max} \sim \cosh^{-2}[(e(C_g/C_\Sigma)|V_{g,peak} - V_{gl})/2.5k_BT]$, with G_{max} and $V_{g,peak}$ being the peak height and position. From such a fit, with a gate capacitance $C_g = 7.5$ aF, derived directly from the oscillation period $\delta V_g = 21$ mV, we obtain a charging energy $E_c = e^2/C_\Sigma \sim 13$ k_BT. Because T should be replaced by the effective electron temperature, which we estimate to be between 25 and 40 mK, we obtain $E_c = 20-45$ μeV, consistent with the half-width of the dips. With increasing T, the Coulomb oscillations are suppressed above 0.3 K, that is, for $k_BT > E_c$. In contrast to the case of **D1**, $E_c \ll \Delta$ implies that many conduction channels become accessible in the NW quantum dot when $E_c \ll eV < \Delta$. This leads to the complete disappearance of the Coulomb-blockade effect in this bias range where transport follows the expectation for a noninteracting SINIS junction.
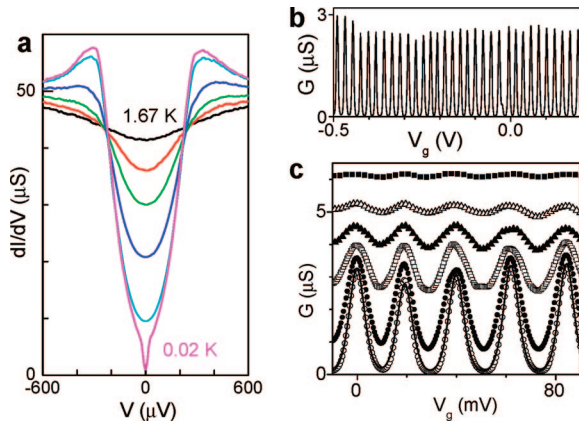
Figure 2. (a) Temperature dependence of differential conductance dI/dV(V) for device **D2** with $B = 0$ mT. From top to bottom: $T =$ 1.67, 1.30, 1.12, 0.84, 0.46, and 0.02 K. The dI/dV peak occurs at $V = \pm 370$ μV at the lowest temperature of $T = 20$ mK. (b) Linear conductance $G(V_g)$ curve at $T = 20$ mK with $B = 0$ mT. (c) T dependence of $G(V_g)$ curve with $T = 20$ (open circle), 70 (closed circle), 140 (open square), 200 (closed triangle), 250 (open triangle), and 310 mK (closed square). The solid line is a fit to the Coulomb oscillations in the classical regime with $k_B T/(e2/C) = 0.076$ (see the text).

To further explore the noninteracting limit down to very low energy scales, we have studied NW devices with $R_N \ll R_Q$, and an always negligible Coulomb energy ($E_c \ll k_B T$). Although $R_N/R_Q \ll 1$ could be obtained with InP NW's of relatively large diameter (see, e.g., device **D3** in Table S1 of the Supporting Information), this low-resistance regime was achieved more efficiently with InAs NWs because of the known ability of this material to form Schottky-barrier-free contacts with metals. A typical magnetoconductance $G(B)$ curve at $T = 30$ mK is shown in the inset of Figure 3a for device **D5**, fabricated from a 80-nm-diameter InAs NW ($L = 110$ nm). The magnetic field was applied perpendicular to the nanowire axis. The NW conductance shows reproducible aperiodic fluctuations with a root-mean square amplitude, rms(G_B) $\equiv$ <($G(B) - <G(B)>)^2>^{1/2}$ = 0.29 and 0.30 e^2/h, for devices **D4** and **D5**, respectively (here angular brackets indicate an average over magnetic field between -5 and 5 T with the exclusion of a 1-T-wide window around zero field where G exhibits an overshoot due to superconductivity as well as possible variations related to weak (anti)localization). These so-called universal conductance fluctuations (UCF) are mesoscopic effects arising from the quantum interference of multiply scattered electronic wave packets.[23] UCFs are known to appear in diffusive conductors when their size is smaller or comparable to the characteristic phase-coherence length, L_ϕ.

An estimate of L_ϕ can be obtained from the autocorrelation function $F(\Delta B) = <G(B)G(B + \Delta B)> - <G(B)>^2$ with ΔB a lag parameter in magnetic field.[24,25] $F(\Delta B)$ is expected to have a peak at $\Delta B = 0$. The half-width at half-height of this peak corresponds to a magnetic correlation length, B_c (conductance values measured at two different fields are uncorrelated when the field difference is much larger than B_c). Figure 3a shows the positive side ($\Delta B > 0$) of the autocorrelation function. From the data obtained in perpen-
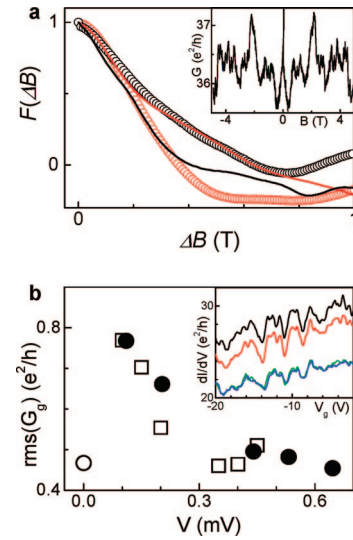

Figure 3. (a) Autocorrelation functions $F(\Delta B)$, extracted from the magnetoconductance $G(B)$ curves at $V_g = 0$ V, for **D4** (red) and **D5** (black) with perpendicular (line) and parallel (circle) magnetic field B to the nanowire axis. The source−drain spacing is $L = 440$ (**D4**) and 110 (**D5**) nm, respectively, and $\phi = 83$ nm. Inset: $G(B)$ curve, obtained from **D5**, with perpendicular B at $T = 30$ mK. The overshoot of G near $B = 0$ T is due to a supercurrent through the nanowire. (b) V-dependent rms(G_g) for devices **D4** (filled circle) and **D6** (square) with $B = 0$ T. For $V = 0$, rms(G_g) = 0.47 e^2/h (open circle) is obtained from **D4** in the normal state with $B = 0.1$ T. Inset: V_g-dependent dynamic conductance curves for **D4** taken at $T = 22$ mK and different bias voltages $V = 0.11$ (black), 0.24 (red), 0.44 (green), and 0.65 (blue) mV.

dicular magnetic field (open dots), we find $B_c = 0.21$ T (**D4**) and 0.18 T (**D5**). According to a theoretical model for quasi-one-dimensional conductors,[26] $B_c = 0.42$ $\Phi_0/(wL_\phi)$, where $\Phi_0 = h/e$ is the one-electron flux quantum and w is the width corresponding to the NW diameter. From $B_c \approx 0.2$ T and $w = 80$ nm, we find $L_\phi \approx 100$ nm. This value is smaller than that obtained from weak localization/antilocalization measurements in similar NWs.[27] Similar $F(\Delta B)$ curves are found for B applied parallel to the NW axis (solid lines in Figure 3a), in contrast with previous results for multiwalled carbon nanotubes.[28] We argue that the seemingly weak dependence of B_c on the field direction reflects the fact that L_ϕ is close to the NW diameter.

UCF have been observed also at $B = 0$ T, using the back-gate voltage as varying parameter (V_g changes the electron density as well as the impurity charge configuration in the nanowire, thereby affecting the quantum interference of scattered electrons). The inset of Figure 3b shows bias-dependent dI/dV(V_g) curves for **D4**. After subtracting the average background conductance obtained from a fit to a second-order polynomial function, we find rms(G_g) = 0.48 $\pm$ 0.02 e^2/h at $V > 2\Delta/e \sim 0.23$ mV. In this large-bias regime, superconducting correlations are expected to vanish similar to the normal-state case discussed above. In the low-bias regime, $V < 2\Delta/e$, the fluctuation amplitude increases substantially (up to a factor 1.6) while its pattern is preserved. We interpret this enhancement of rms(G_g) below the super-conducting gap energy as the result of the correlated interference of additional hole-like quasiparticles generated

in the nanowire by Andreev reflection processes at the contacts, and propagating along the time-reversed path of their electron-like counterparts. An alternative possibility to probe the contribution of Andreev reflection processes is to apply a constant magnetic field that suppresses superconductivity. In the normal-state regime at $B = 0.1$ T, we find rms(G_g)~0.47 e^2/h at $V = 0$, which is close to the high-bias value at $B = 0$. This supports our interpretation in terms of an interplay between UCF and Andreev reflection.

In summary, we have reported the observation of different transport regimes in InP and InAs NWs coupled to superconducting electrodes. The relative weight of Coulomb interactions and Andreev reflection was found to vary from device to device depending on the tunnel coupling strength. Additionally, superconductivity was selectively switched on and off with a moderate magnetic field. In the weak coupling limit, transport occurs via single-electron tunneling due to Coulomb blockade, and negative differential conductance is observed as a result of BCS singularities in the density of states of the electrodes. For strong tunnel coupling, transport is dominated by Andreev reflection, leading to an enhancement of the conductance and its mesoscopic fluctuations. In the intermediate regime, we considered for the first time the case of a Coulomb charging energy much smaller than the superconducting gap. This energy-scale separation results in three clearly distinct regimes: $|V| < E_c$, $E_c < |V| < 2\Delta$, and $|V| > 2\Delta$, fully dominated by Coulomb blockade, Andreev reflection, and noninteracting Ohmic-like transport, respectively. This work emphasizes the potential of semiconductor nanowires as versatile material systems for the investigation of complex fundamental problems involving various competing phenomena such as superconductivity. Along this line, several interesting problems could be addressed in the near future based on the interplay between the superconducting proximity effect and cotunneling,[29] Kondo effect,[11] or Luttinger liquid correlations.[30]

Supporting Information Available: Figure S1: The product of normal state resistance, R_N, and the nanowire-electrode contact area, A, is plotted as a function of the nanowire diameter for InAs (circle) and InP (triangle) nanowires. Figure S2: Differential conductance dI/d$V(V)$ traces for ($\phi = 72$ nm, $L = 220$ nm) at $B = 0$ mT and different temperatures $T = 1.65$ (black), 1.27 (red), 1.10 (green), 0.85 (blue), 0.47 (cyan), and 0.02 K (magenta). Left inset: SEM image of device **D3** (scale bar: 500 nm). Right inset: linear conductance $G(V_g)$ trace in the case of normal-state contacts ($B = 56$ mT). The conductance fluctuations with V_g are reproducible and have an rms amplitude of ~0.4 e^2/h. Table S1: Basic characteristics of the six representative devices discussed in the main text. This material is available free of charge via the Internet at http://pubs.acs.org.

References

(1) Lieber, C. M. *MRS Bulletin* **2003**, *28*, 486.
(2) Samuelson, L.; Björk, M. T.; Deppert, K.; Larsson, M.; Ohlsson, B. J.; Panev, N.; Persson, A. I.; Sköld, N.; Thelander, C.; Wallenberg, L. R. *Phys. E (Amsterdam)* **2004**, *25*, 313.
(3) Björk, M. T.; Ohlsson, B. J.; Thelander, C.; Persson, A. I.; Deppert, K.; Wallenberg, L. R.; Samuelson, L. *Appl. Phys. Lett.* **2002**, *81*, 4458.
(4) De Franceschi, S.; van Dam, J. A.; Bakkers, E. P. A. M.; Feiner, L. F.; Gurevich, L.; Kouwenhoven, L. P. *Appl. Phys. Lett.* **2003**, *83*, 344.
(5) Thelander, C.; Mårtensson, T.; Björk, M. T.; Ohlsson, B. J.; Larsson, M. W.; Wallenberg, L. R.; Samuelson, L. *Appl. Phys. Lett.* **2003**, *83*, 2052.
(6) Zhong, Z.; Fang, Y.; Lu, W.; Lieber, C. M. *Nano Lett.* **2005**, *5*, 1143.
(7) Kouwenhoven, L. P.; Marcus, C. M.; McEuen, P. L.; Tarucha, S.; Westerbelt, R. M.; Wingreen, N. S., Electron transport in quantum dots. In *Mesoscopic Electron Transport*, Sohn, L. L.; Kouwenhoven, L. P.; Schon, G., Eds. Kluwer: Dordrecht, 1997.
(8) Doh, Y.-J.; van Dam, J. A.; Roest, A. L.; Bakkers, E. P. A. M.; Kouwenhoven, L. P.; De Franceschi, S. *Science* **2005**, *309*, 272.
(9) Xiang, J.; Vidan, A.; Tinkham, M.; Westervelt, R. M.; Lieber, C. M. *Nature Nanotechnology* **2006**, *1*, 208.
(10) van Dam, J. A.; Nazarov, Y. V.; Bakkers, E. P. A. M.; De Franceschi, S.; Kouwenhoven, L. P. *Nature* **2006**, *442*, 667.
(11) Sand-Jespersen, T.; Paaske, J.; Andersen, B. M.; Grove-Rasmussen, K.; Jørgensen, H. I.; Aagesen, M.; Sørensen, C. B.; Lindelof, P. E.; Flensberg, K.; Nygård, J. *Phys. Rev. Lett.* **2007**, *99*, 126603.
(12) Ralph, D. C.; Black, C. T.; Tinkham, M. *Phys. Rev. Lett.* **1995**, *74*, 3241.
(13) Whan, C. B.; Orlando, T. P. *Phys. Rev. B* **1996**, *54*, R5255.
(14) Levy Yeyati, A.; Cuevas, J. C.; López-Dávalos, A.; Martín-Rodero, A. *Phys. Rev. B* **1997**, *55*, R6137.
(15) Krstić, V.; Roth, S.; Burghard, M.; Weis, J.; Kern, K. *Phys. Rev. B* **2003**, *68*, 205402.
(16) Shibata, K.; Buizert, C.; Oiwa, A.; Hirakawa, K.; Tarucha, S. *Appl. Phys. Lett.* **2007**, *91*, 112102.
(17) Bakkers, E. P. A. M.; van Dam, J. A.; De Franceschi, S.; Kouwenhoven, L. P.; Kaiser, M.; Verheijen, M.; Wondergem, H.; van der Sluis, P. *Nat. Mater.* **2004**, *3*, 769.
(18) van Houten, H.; Beenakker, C. W. J.; Staring, A. A. M., Coulomb-blockade oscillations in Semiconductor Nanostructures. In *Single Charge Tunneling: Coulomb Blockade Phenomena in Nanostructures*, Grabert, H.; Devoret, M. H., Eds. Plenum Press: New York, 1992.
(19) Likharev, K. K. *IBM J. Res. Dev.* **1988**, *32*, 144.
(20) Dynes, R. C.; Garno, J. P.; Hertel, G. B.; Orlando, T. P. *Phys. Rev. Lett.* **1984**, *53*, 2437.
(21) Kleinsasser, A. W.; Jackson, T. N.; Mclnturff, D.; Rammo, F.; Pettit, G. D.; Woodall, J. M. *Appl. Phys. Lett.* **1990**, *57*, 1811.
(22) Blonder, G. E.; Tinkham, M.; Klapwijk, T. M. *Phys. Rev. B* **1982**, *25*, 4515.
(23) Lee, P. A.; Stone, A. D. *Phys. Rev. Lett.* **1985**, *55*, 1622.
(24) Lee, P. A.; Stone, A. D.; Fukuyama, H. *Phys. Rev. B* **1987**, *35*, 1039.
(25) Al'tshuler, B. L. *Zh. Eksp. Theor. Fiz.* **1985**, *41*, 530.
(26) Beenakker, C. W. J. *Rev. Mod. Phys.* **1997**, *69*, 731.
(27) Hansen, A. E.; Björk, M. T.; Fasth, C.; Thelander, C.; Samuelson, L. *Phys. Rev. B* **2005**, *71*, 205328.
(28) Schönenberger, C.; Bachtold, A.; Strunk, C.; Salvetat, J.-P.; Forro, L. *Appl. Phys. A: Mater. Sci. Process.* **1999**, *69*, 283.
(29) Mkhitaryan, V. V.; Raikh, M. E. *Phys. Rev. B* **2008**, *77*, 195329.
(30) Tilahun, D.; Fiete, G. A. *Phys. Rev. B* **2008**, *77*, R140505.

NL801454K